Pediatric Neurology 94 (2019) 38–47

Contents lists available at ScienceDirect

Pediatric Neurology

journal homepage: www.elsevier.com/locate/pnu

Original Article

Genotypic Spectrum and Natural History of Cavitating Leukoencephalopathies in Childhood

Jie Zhang, MD [a], Ming Liu, MD [a], Zhongbin Zhang, MD [a], Ling Zhou, MD [a], Weijing Kong, MD [a], Yuwu Jiang, MD [a], Jingmin Wang, MD [a], Jiangxi Xiao, MD [b], Ye Wu, MD [a,*]

[a] Department of Pediatrics, Peking University First Hospital, Beijing, China
[b] Department of Radiology, Peking University First Hospital, Beijing, China

ARTICLE INFO

Article history:
Received 4 November 2018
Accepted 1 January 2019
Available online 8 January 2019

Keywords:
Cavitating leukoencephalopathy
Genotype
Natural history
Children

ABSTRACT

Background: We aimed to delineate the pattern of natural course, neuroimaging features, and the genotypic spectrum of cavitating leukoencephalopathies.
Methods: Children (age of onset ≤16 years) who met the criteria for cavitating leukoencephalopathies from January 2009 to October 2018 were identified. Whole-exome sequencing and prospective follow-up study of the natural history and brain magnetic resonance imaging (MRI) were performed.
Results: Thirty-seven children were clinically diagnosed with cavitating leukoencephalopathies. Pathogenic or likely pathogenic mutations in eight genes were identified in 31 individuals (83.78%): *IBA57* (17/37), *NDUFS1* (5/37), *NDUFV1* (2/37), *NDUFV2* (3/37), *NDUFAF5* (1/37), *LYRM7* (1/37), *NDUFB8* (1/37), and *GLRX5* (1/37). All genes were engaged in mitochondrial function. *IBA57* was identified in half of children. Mutations in *NDUFV2*, *NDUFAF5*, *NDUFB8*, or *GLRX5* were first found to be related to cavitating leukoencephalopathies. Follow-up with a median of 23.5 months (four to 107 months) was available. The median age at disease onset was 11 months. All cases presented acute or subacute onset, and the initial presentation was rapid motor regression in 35 cases. Thirty-five children (35/37) exhibited a stabilized or improved pattern. Cavities and high-intensity diffusion-weighted imaging signals were the common MRI features during the acute stage. Although clinically stable, 21 children had reserved high diffusion-weighted imaging signals for a long time. Patients with different gene mutations show different MRI patterns.
Conclusions: The study expands the number of genes involved in cavitating leukoencephalopathies to 22. *IBA57* is the most common candidate gene. Most cases showed a stabilized or improved pattern after an acute or subacute onset, which is different from most other inherited metabolic diseases or leukodystrophies. More cases and a longer follow-up period are needed.

Introduction

Leukodystrophies represent a heterogeneous group of inherited disorders that result in white matter (WM) abnormalities in the central nervous system (CNS).[1] With advancing knowledge of the physiology and pathology, a new classification system of leukodystrophies based on pathologic changes and pathogenic mechanisms was proposed in 2017.[2] WM disorders are classified into myelin disorders (including hypomyelination, demyelination, and myelin vacuolization), astrocytopathies, leukoaxonopathies, microgliopathies, and leukovasculopathies. Some of the leukodystrophies cannot be currently classified pathologically because of the lack of knowledge of their pathogenic mechanisms.

Cavitating leukoencephalopathy (CLE) is an imaging-clinical syndrome that was first proposed in 2005.[3] It was characterized by cavitating lesions in WM and the acute onset of neurological dysfunction. Given its pathologic changes and pathogenetic mechanisms, CLEs would be classified as disorders of myelin vacuolization in new classification system proposed in 2017. CLEs are composed of a group of heterogeneous inherited disorders. We searched the databases including PubMed, OVID, and EMbase, with the key words of “cavitation” or “vacuolization” or “cavity,” and

Conflict of interest: The authors declare that they have no conflict of interest.
* Communications should be addressed to: Dr. Wu; Department of Pediatrics; Peking University First Hospital; Beijing 100034, China.
E-mail address: dryewu@263.net (Y. Wu).

https://doi.org/10.1016/j.pediatrneurol.2019.01.002
0887-8994/

"leukoencephalopathy" or "leukodystrophy." Eighteen genes have been reported to be associated with CLEs until October 2018. These genes are *NDUFV1*[4–6] (MIM 252010), *NUBPL*[7] (MIM 252010), *EFTu*[8] (MIM 610678), *SDHAF1*[9] (MIM 252011), *LRPPRC*[10] (MIM 220111), *COX6B1*[11] (MIM 220110), *NDUFS1*[12,13] (MIM 252010), *NFU1*[14] (MIM 605711), mtDNA*8344A>G*[15] (MIM 545000), *COA7*[16] (MIM 220110), *NOTCH3*[17] (MIM 125310), *LYRM7*[18–20] (MIM 615838), *APOPT1*[21] (MIM 220110), *IBA57*[22–24] (MIM 615330), *SDHA*[25] (MIM 252011), *SDHB*[25] (MIM 252011), *NDUFAF3*[26] (MIM 252010), and *SCO2*[27] (MIM 604272). Except for *NOTCH3*, all these genes are involved in mitochondrial function. Most of descriptions of CLEs were case reports; therefore there is a lack of overall understanding of this group of leukodystrophies. In our study, we performed follow-up with a median of 23.5 months on 37 Chinese children with CLEs. We attempted to delineate the pattern of natural history, neuroimaging characteristics, and the genotypic spectrum.

Patients and Methods

Inclusion and exclusion criteria

Patients who met the following criteria were included: (1) age of onset ≤16 years; (2) acute or subacute onset of neurological dysfunction; and (3) brain magnetic resonance imaging (MRI) in the acute phase (within six months after onset) showing symmetric patchy hyperintensity on T2-weighted imaging (T2WI), T2FLAIR (T2 fluid attenuated inversion recovery), diffusion-weighted imaging (DWI), and hypointensity on T1WI in the periventricular WM and the centrum semiovale. Cavities manifested as fluid-like signals with a clear boundary shown inside the patchy hyperintensity on T2FLAIR imaging. Patients with any of the following criteria were excluded: (1) acquired leukoencephalopathies, including acute disseminated encephalomyelitis, neuromyelitis optica spectrum disorders, multiple sclerosis, CNS vasculitis, and CNS infection; (2) other inherited metabolic diseases as determined through the analysis of amino acids, carnitine, organic acids, and fatty acids.

Genetic analysis

Whole-exome sequencing was performed for the genetic analysis after the inclusion of the patients. The detailed information about the procedures of whole-exome sequencing is given in the supplemental data. The variant classified as "pathogenic" or "likely pathogenic" was selected in accordance with the variant interpretation guidelines of the American College of Medical Genetics and Genomics. Sanger sequencing was performed to validate the variations and determine their parental origin.

Clinical data and follow-up

After the inclusion of the patients, clinical data, including demographic data, developmental milestones, age at disease onset, initial symptoms, and possible precipitating factors were collected at first visit. A prospective follow-up with a median of 23.5 months (four to 107 months) after the first visit was conducted through outpatient visits, telephone queries, and electronic questionnaires. We used the Gross Motor Function Classification System (GMFCS) to assess motor function. Motor function was divided into I to V levels. A higher level indicated a greater limitation of motor function. Ages and Stages Questionnaires-Chinese (ASQ-C) and Adaptive Behavior Assessment System II (ABAS-II) were used to evaluate cognitive function. All the questionnaires were performed by their parents. ASQ-C (age ranging from one month to 66 months) consisted of 30 items that assessed development in the areas of gross motor, fine motor, communication, problem solving, and personal-social skills. We focused on the last three items for cognitive assessments. ABAS-II (age ≥6 years) assessed development in the areas of comprehensive adaptability, conceptual skills, social skills, and practical skills.

Analysis of brain MRI

Brain MRIs were analyzed in the peak and recovery phases after onset, respectively. Peak phase was defined as the phase when the brain MRI showed the widest range of high signals on DWI and within six months of onset. Recovery phase was defined as the latest brain MRI during the follow-up, and at least six months after onset. We evaluated the extent of WM lesions, cavities, diffusion-restricted lesions, and atrophy. Lesions were defined as areas that were hyperintense on T2WI and hypointense on T1WI. Cavities were defined as areas that were hyperintense on T2WI and hypointense on T2FLAIR. Diffusion-restricted lesions were identified as areas with high-intensity signals on DWI.

Standard protocol approval and patient consents

The study was approved by the clinical research ethics committee of the Peking University First Hospital. Written informed consents were obtained from the parents.

Statistical analysis

After the patients with different disease-causing genes were grouped, the clinical data, natural course, and brain MRI were analyzed and compared. Medians were used to describe their average and variability. The measurement or ranked data of each group were described using cases and percentages. Hypothesis testing and statistical comparison among the different groups were not performed because of the small number of cases in each group. Data processing and statistical analysis were performed using Statistical Product and Service Solutions 20.0.

Results

Eight disease-causing genes identified

From January 2009 to October 2018, 37 children (19 males, 18 females) from 35 families were clinically diagnosed with CLEs in Peking University First Hospital, including three pairs of siblings. In 31 patients, pathogenic/likely pathogenic variants either compound heterozygous or homozygous in eight genes were identified. They were *IBA57* (encoding IBA57 homolog, iron-sulfur cluster assembly) (17/37,45.9%), *NDUFS1* (NADH:ubiquinone oxidoreductase core subunit S1) (5/37,13.5%), *NDUFV1* (NADH:ubiquinone oxidoreductase core subunit V1) (2/37, 5.4%), *NDUFV2* (NADH:ubiquinone oxidoreductase core subunit V2) (3/37, 8.1%), *NDUFAF5* (NADH:ubiquinone oxidoreductase complex assembly factor 5) (1/37, 2.7%), *LYRM7* (LYR motif containing 7) (1/37, 2.7%), *NDUFB8* (NADH:ubiquinone oxidoreductase subunit B8) (1/37, 2.7%), and *GLRX5* (glutaredoxin 5) (1/37, 2.7%) (Table 1).

Description of two typical patients

Patient 19: This girl developed normally until age 21 months, then presented with rapid motor regression two days after a respiratory infection. The deterioration of neurological function reached its nadir after three days and she completely lost the skills of walking and sitting. Her motor function was classified as GMFCS V at the nadir. Physical examination at the first visit showed rigidity, brisk reflexes, and Babinski signs. Lactic acid in blood was

TABLE 1.
Genotypes and Phenotypes of the 37 Children With Clinically Diagnosed CLEs

Case	Sex	Age of Onset (mon)	Pattern of Disease Course	Pattern of Brain MRI	Gene	Nucleotide Change	Amino Acid Change	Novel/ Reported	Parental Derivation	Interpretation according to ACMG Criteria
1	M	13	S	Di	*IBA57*	c.286T>C	p.Tyr96His	R	Pa	LP
						c.697C>T	p.Arg233X	R	M	P
2	F	9	S	De	*IBA57*	c.286T>C	p.Tyr96His	R	Pa	LP
						c.316A>G	p.Thr106Ala	R	M	LP
3	F	15	S	Di	*IBA57*	c.286T>C	p.Tyr96His	R	Pa	LP
						c.316A>G	p.Thr106Ala	R	M	LP
4	M	5	S	Di	*IBA57*	c.286T>C	p.Tyr96His	R	Pa	LP
						c.697C>T	p.Arg233X	R	M	P
5	F	9	S	De	*IBA57*	c.22C>T	p.Arg8X	R	Pa	P
						c.286T>C	p.Tyr96His	R	M	LP
6	F	18	S	Di	*IBA57*	c.286T>C	p.Tyr96His	R	M	LP
						c.307C>T	p.Gln103X	R	Pa	P
7	M	16	S	De	*IBA57*	c.286T>C	p.Tyr96His	R	M	LP
						c.307C>T	p.Gln103X	R	Pa	P
8	M	9	S	Di	*IBA57*	c.286T>C	p.Tyr96His	R	Pa	LP
						c.754G>T	p.Gly252Cys	R	M	LP
9	M	10	S	Di	*IBA57*	c.286T>C	p.Tyr96His	R	M	LP
						c.697C>T	p.Arg233X	R	Pa	P
10	F	5	S	Di	*IBA57*	c.701A>G	p.Asp234Gly	R	M	LP
						c.782T>C	p.Ile261Thr	R	Pa	LP
11	F	9	S	De	*IBA57*	c.286T>C	p.Tyr96His	R	*De novo*	LP
						c.697C>T	p.Arg233X	R	M	P
12	M	5	S	Di	*IBA57*	c.286T>C	p.Tyr96His	R	Pa	LP
						c.188G>A	p.Gly63Asp	N	M	LP
13	M	11	S	De	*IBA57*	c.286T>C	p.Tyr96His	R	M	LP
						c.1053G>A	p.Trp351X	N	Pa	P
14	F	11	S	Di	*IBA57*	c.588_589del	p.Arg197AlafsTer6	N	M	P
						c.286T>C	p.Tyr96His	R	Pa	LP
15	M	8	S	Di	*IBA57*	c.522_523del	p.Ser174SerfsTer29	N	M	P
						c.286T>C	p.Tyr96His	R	Pa	LP
16	F	9	S	Di	*IBA57*	c.307C>T	p.Gln103X	R	M	P
						c.236C>T	p.Pro79Leu	N	Pa	LP
17	F	11	S	Di	*IBA57*	c.188G>A	p.Gly630Asp	N	M	LP
						c.286T>C	p.Tyr96His	R	Pa	P
18	F	15	S	Di	*NDUFS1*	c.1552delA	p.Arg518GlyfsTer6	N	M	P
						c.1102A>C	p.Thr368Pro	N	Pa	LP
19	F	21	S	Di	*NDUFS1*	c.1256G>A	P.Arg419Gln	N	M	LP
						c.627C>A	p.Tyr209X	N	Pa	P
20	F	7	S	De	*NDUFS1*	c.1612G>C	p.Ala538Pro	N	Pa	LP
						c.1852C>T	p.Gln618X	N	M	P
21	M	5	Pr	Di	*NDUFS1*	c.106G>T	p.Val36Phe	N	M	LP
						c.908A>T	p.Lys303Ile	N	Pa	LP
22	F	6	S	Di	*NDUFS1*	c.1721A>T	P.Asp574Val	N	Pa	LP
						c.1458_1459insTGGA	p.Asp574ValfsTer10	N	M	P
23	M	3	Pr	Di	*NDUFV1*	c.248C>T	p.Ser83Leu	N	M	LP
						c.365C>T	p.Pro122Leu	R	Pa	LP
24	M	7	S	De	*NDUFV1*	c.652G>T	p.Gly218Cys	N	Pa	LP
						c.1117T>C	p.Phe373Leu	N	M	LP
25	M	12	S	Fr	*NDUFV2*	c.404G>C	p.Cys135Ser	R	M	P
						c.467T>A	p.Leu156His	R	Pa	P
26	M	4	S	Fr	*NDUFV2*	c.404G>C	p.Cys135Ser	R	M	P
						c.467T>A	p.Leu156His	R	Pa	P
27	M	46	S	De	*NDUFV2*	c.62_63del	p.His21ArgfsTer6	N	Pa	P
						c.694A>C	p.Thr232Pro	N	M	LP
28	F	6	S	Mu	*NDUFAF5*	c.508C>T	p.Arg170Trp	N	M	LP
						c.764C>T	p.Ala255Val	N	Pa	LP
29	F	6	S	De	*LYRM7*	c.243_244 + 2del	Splicing mutation	R	M	P
						c.243_244 + 2del	Splicing mutation	R	Pa	P
30	F	10.5	S	Mu	*NDUFB8*	c.227C>T	p.Pro76Leu	N	Pa (UPD)	LP
						c.227C>T	p.Pro76Leu	N	Pa (UPD)	LP
31	F	14	S	Di	*GLRX5*	c,151_153delAAG	p.Lys51del	R	M	LP
						c.196C>T	p.Gln66X	N	Pa	LP
32	M	15	S	De	-	-	-	-	-	-
33	M	14	S	De	-	-	-	-	-	-
34	F	32	S	Mu	-	-	-	-	-	-

(*continued on next page*)

TABLE 1. (*continued*)

Case	Sex	Age of Onset (mon)	Pattern of Disease Course	Pattern of Brain MRI	Gene	Nucleotide Change	Amino Acid Change	Novel/ Reported	Parental Derivation	Interpretation according to ACMG Criteria
35	F	15	S	Mu	-	-	-	-	-	-
36	M	13	S	De	-	-	-	-	-	-
37	M	32	S	De	-	-	-	-	-	-

Abbreviations:
ACMG = American College of Medical Genetics and Genomics
CLE = Cavitating leukoencephalopathy
De = Deep WM pattern;
Di = Diffused WM pattern
Fr = Frontal predominant pattern
LP = Likely pathogenic
M = Maternal
MRI = Magnetic resonance imaging
Mu = Multiple-lesion pattern
N = Novel
Pa = Paternal
P = Pathogenic
Pr = Progressively deteriorated pattern
R = Reported
S = Stabilized/improved pattern
UPD = Uniparental disomy
WM = White matter
- = Not identified

normal, and the hepatic and renal function tests were also normal. Brain MRI at the peak phase (one month after disease onset) is shown in Fig 1 (B1-B4). The motor function gradually improved after three months. At her last follow-up visit at age three years and five months (20 months after disease onset), she could walk and sit independently, and the motor function was classified as GMFCS I. The cognitive function was also normal. The MRI at the recovery phase (14 months after disease) showed shrinkage of the WM lesions and cavities. The extent of high DWI signals also significantly decreased. Finally, c.1256G>A (p. Cys135Ser) and c.627C>A (p. Tyr209X) mutations in the *NDUFS1* were identified.

Patient 26: This boy was the second child of healthy, unrelated parents. He had a brother with similar symptoms. The boy developed normally before age four months, when he developed motor regression without obvious preceding factors. His deterioration of neurological function reached its nadir after one month and he could not laugh responsively, raise head, or roll over. The motor function was classified as GMFCS V. Brain MRI at the peak phase (three months after disease onset) is shown in Fig 1 (F1-F4). His motor and intellectual function developed slowly during the 9.5 years of follow-up. At the last follow-up, when he was nine years and 10 months, he could walk independently for a short distance, but his fine motor movement was relatively poor. The motor function was classified as GMFCS II. The cognitive function was moderately below the normal level. The WM lesions, cavities, and high DWI signals completely disappeared, and the atrophy of the WM in the frontal and parieto-occipital lobes was found in the MRI at the recovery phase (eight years and two months after disease onset). c.404G>C (p. Arg419Gln) and c.467T>A (p. Leu156His) mutations in the *NDUFV2* were identified in him and his younger brother.

Natural history

Disease onset

Most patients (25/37, 67.6%) developed normally before disease onset, whereas in 32.4% (12/37) there was mild delay. The median age at onset was 11 months (three to 46 months). Twenty-one of 37 (56.76%) patients experienced a respiratory infection several days before the onset. The median time at which the deterioration of neurological function reached its nadir was one month (three days to four months). Initial symptom was motor regression in most patients (35/37, 94.6%), whereas seizures in two (5.4%). At the first visit, with the median four months (one to 83 months) after disease onset, 91.9% (34/37) showed abnormal physical signs, including rigidity (91.9%, 34/37), brisk reflexes (86.5%, 32/37), and Babinski signs (75.7%, 28/37).

Evolution of symptoms during disease course

After the first visit, follow-up with a median of 23.5 months (four to 107 months) was available. The age at the last follow-up was 50 months (15 to 143 months), with the median disease course 34 months (five to 134 months). At the last follow-up, 35 patients survived with stable conditions, and two children died. One patient with mutations in *NDUFS1* died at age 15 months (10 months after disease onset), and the other with mutations in *NDUFV1* died at age six years (64 months after onset).

Motor function. All cases were classified as GMFCS V at the nadir. At the last follow-up, seven patients had followed up less than one year after disease onset and one patient died; the motor function of other six patients was classified as GMFCS IV to V (50.0%, 3/6), GMFCS III (16.7%, 1/6), and GMFCS I to II (33.3%, 2/6). Twenty-three patients had followed up between one to five years after disease onset, the motor function was classified as GMFCS IV to V (30.4%, 7/23), GMFCS III (30.4%, 7/23), and GMFCS I to II (39.1%, 9/23). Seven patients had followed up more than five years, except one patient died, most of the patients showed great improvement in motor function, GMFCS I to II was in 83.3% (5/6), whereas GMFCS IV to V in only 16.7% (1/6).

Cognitive function. ASQ-C was completed in 27 children younger than 66 months at the last follow-up. The results indicated that 48.2%, 55.6%, and 59.3% were delayed in communication, problem solving, and personal-social skills. Other four cases ≥6-year old at the last follow-up were evaluated by ABAS-II, of which two individuals (50.0%, 2/4) exhibited delayed social skills, one (25.0%, 1/4) showed delayed conceptual skills, and all (100%, 4/4) had delayed general adaptation and practical skills.

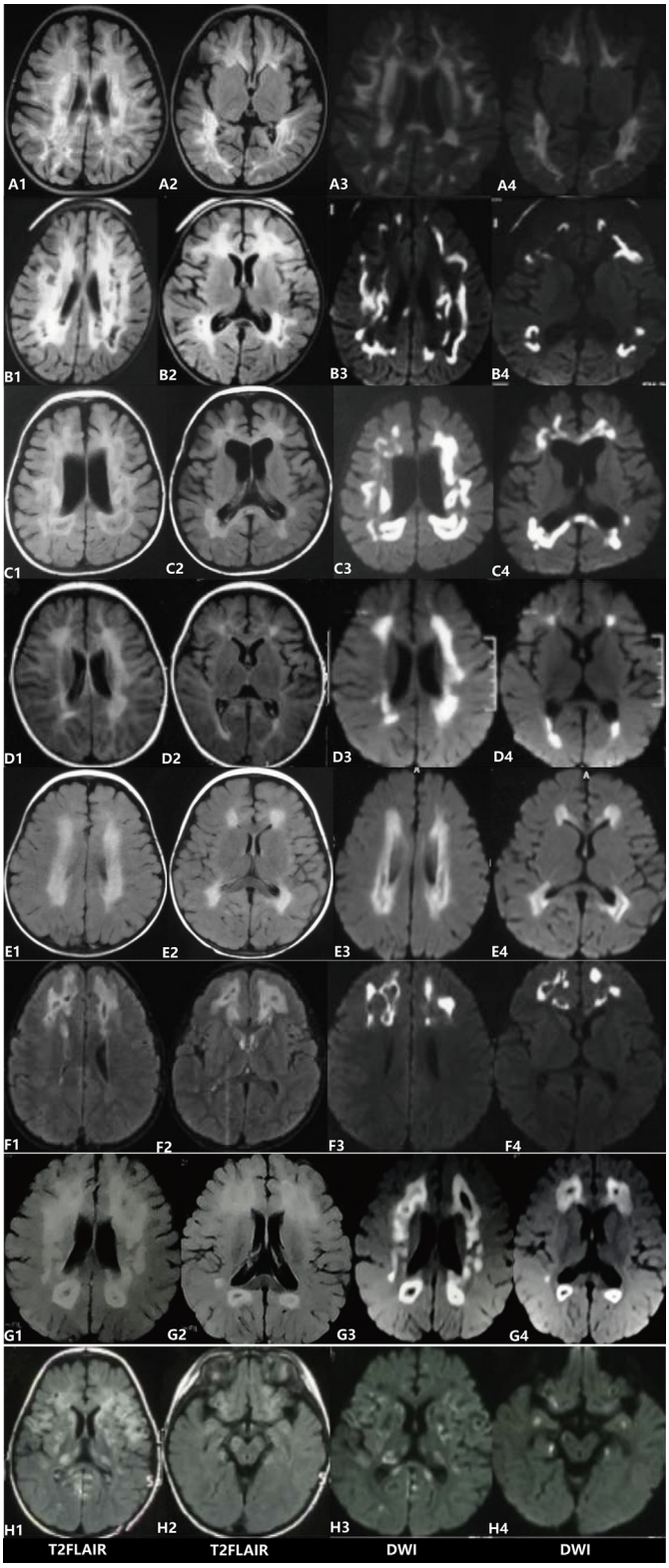

FIGURE 1. MRI in patients with different mutant genes. (A1-C4) *Diffuse WM pattern*: MRI of the patients with *IBA57* (A1-A4, Patient 12), *NDUFS1* (B1-B4, Patient 19), and *GLRX5* (C1-C4, Patient 31) mutations at the peak phase exhibiting periventricular and subcortical hyperintensity in the frontal, parieto-occipital, and temporal lobes on T2FLAIR (A1-A2, B1-B2, and C1-C2) and DWI (A3-A4, B3-B4, and C3-C4). Cavities were observed in the periventricular WM. (D1-E4) *Deep WM pattern*: MRI of the patients with *NDUFV1* (D1-D4, Patient 24) and *LYRM7* (E1-E4, Patient 29) mutations at the peak phase exhibiting periventricular hyperintensity in the frontal and parieto-occipital lobes on T2FLAIR (D1-D2 and E1-E2) and DWI (D3-D4 and E3-E4) without the involvement of subcortical WM. Cavities were observed in the periventricular WM on T2FLAIR. (F1-F4) *Frontal prominent pattern*: MRI of Patient 26 with *NDUFV2* mutations at the peak phase exhibiting periventricular hyperintensity in the frontal lobes on T2FLAIR (F1-F2) and DWI (F3-F4). Cavities were observed in the periventricular WM in the frontal lobes on T2FLAIR. (G1-H4) *Multiple-lesion pattern*: MRI of the patients with *NDUFB8* (G1-G4, Patient 30) and *NDUFAF5* (H1-H4, Patient 28) mutations at the peak phase exhibiting periventricular and subcortical hyperintensity in the frontal and parieto-occipital lobes on T2FLAIR (G1-G2 and H1-H2) and DWI (G3-G4 and H3-H4). Cavities were observed in the periventricular WM on T2FLAIR. Corpus callosum, brainstem, basal ganglia, thalamus, and cerebellum were involved. DWI = Diffusion-weighted imaging; MRI = Magnetic resonance imaging; WM = White matter. The color version of this figure is available in the online edition.

Other neurological dysfunction. Although relatively stable, there were mild fluctuations of motor functions in the case of infectious disease in 32.4% (12/37) of the cases. During the follow-up, visual impairment occurred in 12 cases (32.4%), followed by epilepsy (11/37, 29.7%). Patients with *IBA57* mutations had a higher risk of visual impairment (47.1%, 8/17). Visual impairment was found 0.5 to 32.0 months after disease onset, with 62.5% (5/8) within the first year. Other common clinical manifestations, such as myopathy and deafness, were not present in any patient.

Other investigations. Hyperlactacidemia (2.2 to 10.2 mmol/L) was identified in 56.0% (14/25) of the cases. Hepatic and renal function tests were normal in all cases. No patient exhibited myocardial hypertrophy during the follow-up.

Features of brain MRI

A total of 117 brain MRI scans were collected (one to eight times per case). MRI in the peak period was performed at an average of two months (0.5 to 6.0 months) after disease onset, and 25 cases underwent MRI in the recovery phase at an average of 26.0 months (6.0 to 55.0 months) after disease onset (Fig 2).

Evolution of WM abnormalities during disease course. The acute stage was characterized by well-defined patchy T1WI hypointensity and T2WI hyperintensity as well as T2WI hyperintensity and T2FLAIR hypointensity with clear boundary representing cavities. T1WI hypointensity or T2WI hyperintensity predominated in the deep WM of the frontal (100%, 37/37) and parieto-occipital (97.3%, 36/37) lobes. They also occur in the WM of the temporal lobes, corpus callosum, internal capsule, basal ganglia, thalamus, brainstem, and cerebellum. Cavities predominantly formed in the deep WM of the frontal (86.5%, 32/37) and parieto-occipital (97.3%, 36/37) lobes, but can also occur in the temporal lobes, corpus callosum, thalamus and cerebellum. Patchy DWI high-intensity signals were predominantly observed in the deep WM of the frontal (100%, 37/37) and parieto-occipital (97.3%, 36/37) lobes. They also occurred in the WM of the temporal lobes, corpus callosum, internal capsule, basal ganglia, thalamus, brainstem, and cerebellum (Table 2).

In the recovery stage, the WM lesions and cavities shrunk in 68.0% (17/25) of the cases. High DWI signals disappeared in only four cases (16.0%, 4/25). In the remaining 21 cases with reserved high DWI signals, 61.9% (13/21) exhibited a remarkable decrease, whereas 38.1% (8/21) presented new stippled or linear high DWI signals that differed from the original lesions. Atrophy of the WM was common, involved in frontal lobes, parieto-occipital lobes, temporal lobes, and corpus callosum as well.

Features of brain MRI in different CLEs. We divided the MRI at the peak phase into four categories on the base of the extent of WM lesions: (1) *diffuse WM pattern*: MRI showed diffuse lesions involving both the deep and subcortical WM; (2) *deep WM pattern*: the lesions limited in the deep WM; (3) *frontal predominant pattern*: the prominent lesions were located in the WM of frontal lobes; (4) *multiple-lesion pattern*: multiple regions were involved, including the WM of frontal and parieto-occipital lobes, corpus callosum, brainstem, internal capsule, basal ganglia, and thalamus.

There are slight differences in CLEs with different mutant genes. The patients with *IBA57*, *NDUFS1*, *NDUFV1*, and *GLRX5* mutations

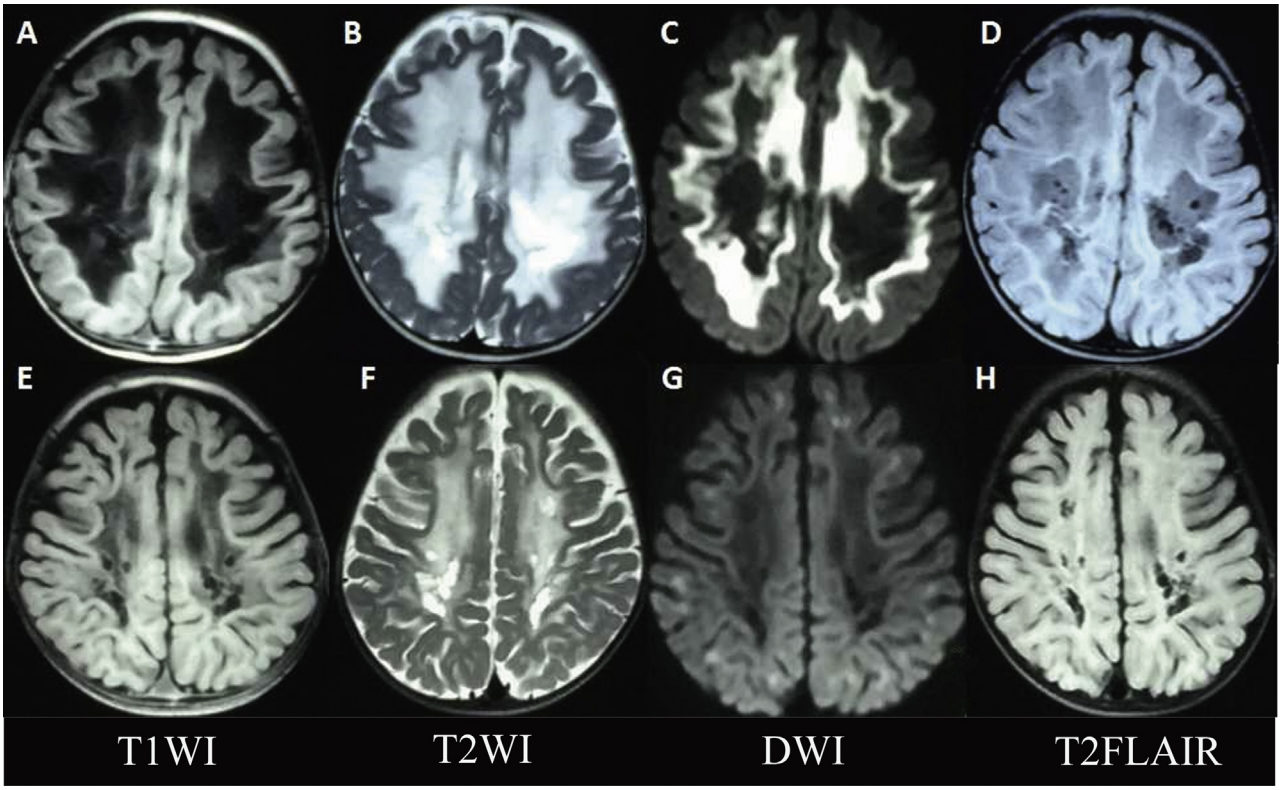

FIGURE 2. MRI at the peak and recovery stage. (A-D) MRI of Patient 22 at the peak phase exhibiting periventricular and subcortical hypointensity on T1WI (A) and hyperintensity on T2WI (B), T2FLAIR (D), and DWI (C). Cavities were observed on T2FLAIR (D). (E-H) MRI of Patient 22 at the recovery phase exhibiting periventricular and central hypointensity on T1WI (E) and hyperintensity on T2WI (F) and T2FLAIR (H). Range of lesions and cavities showed considerable decrease in size. Hyperintensity on DWI (G) significantly decreased, but incompletely disappeared. DWI = Diffusion-weighted imaging; MRI = Magnetic resonance imaging; T1WI = T1-weighted imaging; T2WI = T2-weighted imaging. The color version of this figure is available in the online edition.

TABLE 2.
Brain MRI Features in the Acute Stage of the 37 Children With Clinically Diagnosed CLEs

Location	Lesion (%)	Cavity (%)	DWI High-Intensity Signal (%)	Atrophy (%)
Acute stage				
Frontal lobes				0.0% (0/37)
Deep WM	100.0% (37/37)	86.5% (32/37)	100% (37/37)	
Subcortical WM	51.4% (19/37)	0.0% (0/37)	40.5% (15/37)	
Temporal lobes				0.0% (0/37)
Deep WM	56.8% (21/37)	13.5% (5/37)	51.4% (19/37)	
Subcortical WM	5.4% (2/37)	0.0% (0/37)	5.4% (2/37)	
Parieto-occipital lobes				0.0% (0/37)
Deep WM	97.3% (36/37)	97.3% (36/37)	97.3% (36/37)	
Subcortical WM	40.5% (15/37)	0.0% (0/37)	35.1% (13/37)	
Corpus callosum	73.0% (27/37)	16.2% (6/37)	70.3% (26/37)	0.0% (0/37)
Brainstem	13.5% (5/37)	0.0% (0/37)	13.5% (5/37)	0.0% (0/37)
Internal capsule	21.6% (8/37)	0.0% (0/37)	18.9% (7/37)	0.0% (0/37)
Basal ganglia	5.4% (2/37)	0.0% (0/37)	2.7% (1/37)	0.0% (0/37)
Thalamus	10.8% (4/37)	2.7% (1/37)	10.8% (4/37)	0.0% (0/37)
Cerebellum	16.2% (6/37)	5.4% (2/37)	13.5% (5/37)	0.0% (0/37)
Recovery stage				
Frontal lobes				88.0% (22/25)
Deep WM	96.0% (24/25)	76.0 (19/25)	68.0% (17/25)	
Subcortical WM	24.0% (6/25)	0.0% (0/25)	24.0% (6/25)	
Temporal lobes				44.0% (11/25)
Deep WM	64.0% (16/25)	4.0% (1/25)	40.0% (10/25)	
Subcortical WM	4.0% (1/25)	0.0% (0/25)	8.0% (2/25)	
Parieto-occipital lobes				100.0% (25/25)
Deep WM	100.0% (25/25)	88.0% (22/25)	52.0% (13/25)	
Subcortical WM	24.0% (6/25)	0.0% (0/25)	16.0% (4/25)	
Corpus callosum	72.0% (18/25)	16.0% (4/25)	28.0% (7/25)	44.0% (11/25)
Brainstem	12.0% (3/25)	0.0% (0/25)	16.0% (4/25)	0.0% (0/25)
Internal capsule	28.0% (7/25)	0.0% (0/25)	16.0% (4/25)	0.0% (0/25)
Basal ganglia	4.0% (1/25)	4.0% (1/25)	4.0% (1/25)	0.0% (0/25)
Thalamus	4.0% (1/25)	4.0% (1/25)	4.0% (1/25)	0.0% (0/25)
Cerebellum	12.0% (3/25)	4.0% (1/25)	12.0% (3/25)	0.0% (0/25)

Abbreviations:
DWI = Diffusion-weighted imaging
CLE = Cavitating leukoencephalopathy
MRI = Magnetic resonance imaging
WM = White matter

tended to show the diffuse WM pattern. The deep WM patterns were shown in patients with *IBA57*, *NDUFS1*, *NDUFV1*, *NDUFV2*, and *LYRM7* mutations. MRIs in the patients with *NDUFV2* mutations tended to manifest the frontal predominant pattern. Multiple-lesion pattern was shown in the cases with *NDUFAF5* and *NDUFB8* mutations (Table 3 and Fig 1).

Discussion

CLEs refer to a group of heterogeneous genetic disorders sharing similar neuroimaging features characterized by cavities in WM in the acute phase. Pathology findings of CLE from biopsy data from one patient and autopsy data from three patients (10 months, 2.3 years and 7.2 years after disease onset, respectively) included pallor and loosening of the neuropil, with the loss of normal myelin staining, and oligodendrocytes disappeared because of axonal disruption in the lesions, and cavity.[3] These findings suggest that CLE should be classified as a myelin vacuolization disorder as proposed in the classification system of leukodystrophies in 2017.

Most of genes causing CLEs are involved in mitochondrial function

Eighteen genes have been previously reported to be associated with CLE. In the present study, we identified mutations in eight genes in 31 of 37 children with clinically diagnosed CLE, including *IBA57*, *NDUFS1*, *NDUFV1*, *NDUFV2*, *NDUFAF5*, *LYRM7*, *NDUFB8*, and *GLRX5*. Mutations in *IBA57* were found in half of patients; therefore it is the most common disease-causing gene in CLEs. Among the eight genes, four were found to result in CLEs for the first time, they were *NDUFV2*, *NDUFAF5*, *NDUFB8*, and *GLRX5*. A Leigh syndrome phenotype was previously reported in patients with *NDUFAF5*,[28] *NDUFB8*,[29] *NDUFV2*,[30,31] and *SCO2*[32] mutations, with the brain lesions limited in the bilateral basal ganglia, thalamus, and brainstem. Hypertrophic cardiomyopathy was also reported in cases with *NDUFV2*[30,31] and *SCO2*[32] mutations previously. The previously reported phenotypes of patients with *GLRX5* mutations were sideroblastic anemia and childhood onset hyperglycinemia with spasticity.[33]

Among the 22 genes related to CLEs, all are involved in mitochondrial function except for *NOTCH3*. These genes encode proteins of core subunits of mitochondrial membrane respiratory chain complex (*NDUFS1*, *NDUFV1*, *NDUFV2*, *NDUFB8*, *SDHA*, *SDHB*, *COX6B1*, and *APOPT1*), the assembly factors (*NDUFAF5*, *NUBPL*, *NDUFAF3*, *SDHAF1*, *LYRM7*, *COA7*, and *SCO2*), and the iron-sulfur cluster assembly pathway (*NFU1*, *IBA57*, and *GLRX5*). *EFTu* encodes a protein that is the mitochondrial translation elongation factor, and *LRPPRC* encodes a leucine-rich protein that has multiple pentatricopeptide repeats, which might play a role in cytoskeletal organization, vesicular transport, or transcriptional regulation of both nuclear and mitochondrial genes. On the basis of the functions of the genes, CLEs are probably resulted from the dysfunction of energy metabolism in the mitochondria; therefore majority of CLEs are mitochondrial leukoencephalopathies.

Neuroimaging features of CLEs have similarities, but also differences

The most common feature of brain MRI was the WM cavities according to the proposed criteria of CLE. The lesions and cavities in

TABLE 3.
Brain MRI Patterns of the Patients With Different Gene Mutations

MRI Patterns				
Genes	Diffused WM Pattern	Deep WM Pattern	Frontal Predominant Pattern	Multiple-Lesion Pattern
IBA57	70.6% (12/17)	29.4% (5/17)	0.0% (0/17)	0.0% (0/17)
NDUFS1	80.0% (4/5)	20.0% (1/5)	0.0% (0/5)	0.0% (0/5)
NDUFV1	50.0% (1/2)	50.0% (1/2)	0.0% (0/2)	0.0% (0/2)
NDUFV2	0.0% (0/3)	33.3% (1/3)	66.7% (2/3)	0.0% (0/3)
NDUFAF5	0.0% (0/1)	0.0% (0/1)	0.0% (0/1)	100% (1/1)
LYRM7	0.0% (0/1)	100% (1/1)	0.0% (0/1)	0.0% (0/1)
NDUFB8	0.0% (0/1)	0.0% (0/1)	0.0% (0/1)	100% (1/1)
GLRX5	100% (0/1)	0.0% (0/1)	0.0% (0/1)	0.0% (0/1)
Negative	0.0% (0/6)	66.7% (4/6)	0.0% (0/6)	33.3% (2/6)

Abbreviations:
MRI = Magnetic resonance imaging
WM = White matter

the acute phase were prominent in the WM of centrum semiovale and also involved the subcortical WM in a few cases. High-intensity DWI signal indicating cytotoxic edema or myelin edema, which was rarely mentioned in previously reported CLEs, was another common feature in our cases (100%). High-intensity DWI signals tended to locate in the surrounding regions around the cavities.

In the recovery stage, the extent of lesions and cavities were gradually reduced, accompanied with the atrophy of WM. However, high-intensity DWI signals did not completely disappear in most cases even with a median of 24.0 months' follow-up. A total of 61.9% of cases exhibited high-intensity DWI signals in the original lesions, whereas 38.1% presented new stippled or linear high DWI signals that differed from the original lesions without clinical manifestations of relapses.

Brain MRIs from children with different mutant genes showed some differences. Totally, 76 genetically diagnosed patients, 45 cases from the previous literature, and 31 cases from our study were collected. We categorized the WM lesions into several patterns, including the diffuse WM pattern, deep WM pattern, frontal predominant pattern, parieto-occipital predominant pattern, and multiple-region pattern. The brain MRI patterns of the patients with different mutant genes are shown in Table 4. The previous reported patients with *NOTCH3*[17] mutations manifested another special pattern with subcortical infarcts and cavities related to blood vessel. Because of the small number of the cases with each mutant gene, the MRIs showed the heterogeneous features. For example, the patients with *IBA57*, *NDUFS1*, *NDUFV1*, and *LRPPRC* mutations showed two different patterns, the diffuse and deep WM

TABLE 4.
Brain MRI and Disease Course Patterns of the Patients With Different Gene Mutations (Including the Patients From the Previous Literature)

Patterns									
Genes	Total Cases (n)	Brain MRI Patterns					Disease Course Patterns		
		Diffuse WM Pattern (n)	Deep WM Pattern (n)	Frontal Predominant Pattern (n)	Parieto-occipital Predominant Pattern (n)	Multiple-Region Pattern (n)	Stabilized/ Improved Pattern (n)	Progressive Deterioration Pattern (n)	Paroxysmal Deterioration Pattern (n)
NUBPL	1[7]	-	-	1	-	-	-	-	1
EFTu	1[8]	1	-	-	-	-	-	-	1
SDHAF1	1[9]	-	1	-	-	-	1	-	-
LRPPRC	1[10]	-	-	-	-	1	-	-	1
COX6B1	2[11]	-	2	-	-	-	1	1	-
mtDNA8344A>G	1[15]	-	1	-	-	-	-	-	-
COA7	1[16]	-	-	-	1	-	1	-	-
APOPT1	6[21]	-	1	-	5	-	6	-	-
NFU1	1[14]	-	1	-	-	-	-	-	1
SDHA	1[25]	-	1	-	-	-	1	-	-
SDHB	1[25]	-	1	-	-	-	1	-	-
NDUFAF3	1[26]	-	-	-	-	1	1	-	-
SCO2	1[27]	-	1	-	-	-	1	-	-
IBA57	7[22–24]	2	5	-	-	-	5	2	-
	17	*12*	*5*	-	-	-	17	-	-
NDUFS1	3[4,12,13]	1	2	-	-	-	3	-	-
	5	*4*	*1*	-	-	-	*4*	*1*	-
NDUFV1	5[4–6]	5	-	-	-	-	5	-	-
	2	*1*	*1*	-	-	-	*1*	*1*	-
NDUFV2	*3*	-	*1*	*2*	-	-	*3*	-	-
NDUFAF5	*1*	-	-	-	-	*1*	*1*	-	-
LYRM7	10[18–20]	1	9	-	-	-	4	-	6
	1	-	*1*	-	-	-	*1*	-	-
NDUFB8	*1*	-	-	-	-	*1*	1	-	-
GLRX5	*1*	*1*	-	-	-	-	*1*		
NOTCH3	1[17]	-	-	-	-	-	-	-	-

Abbreviations:
MRI = Magnetic resonance imaging
n = The number of cases
WM = White matter
- = Not identified
The italic numbers represent the number of cases in our study.

patterns. The patients with *NDUFV2* mutations showed the frontal predominant or deep WM patterns. Brainstem (*IBA57*, *APOPT1*, *SDHAF1*, *NDUFB8*, and *NDUFAF5* mutations), cerebellum (*NDUFS1*, *NDUFAF5*, *LYRM7*, and *NUBPL* mutations), thalamus (*EFTu*, *LYRM7*, *NDUFB8*, *NDUFAF3*, *SCO2*, and *NDUFAF5* mutations), and the basal ganglia (*NDUFB8* and *NDUFAF5* mutations) were involved in the acute stage in some of CLEs.

Different patterns of disease course in CLEs

We classified the disease course into three patterns (including the previous reports and our cases in the present study) on the basis of clinical evolution after disease onset, with the median follow-up 3.25 years (four months to 22 years): (1) *Stabilized/improved pattern*: the children had only one episode. After the acute or subacute episode, they remained stable or even showed great improvement. Most children of CLEs presented with this pattern. This differs from other inherited metabolic diseases and most of other leukodystrophies, which are usually progressive. Some of these patients showed mild fluctuation during infectious illnesses during the follow-up. (2) *Progressively deteriorated pattern*: a few patients exhibited rapidly progressive deterioration after disease onset and died within a few months. (3) *Paroxysmal deterioration pattern*: a few reported patients presented with recurrent paroxysmal aggravations in the case of infectious disease, and with gradual deterioration. The disease course patterns of the patients with different mutant genes are shown in Table 4.

It is interesting that the stabilized/improved pattern (one-episode only pattern) is the most common pattern in these mitochondrial leukoencephalopathies. We hypothesized that the higher demand for energy to synthesize protein for myelination in the developing brain could induce a decompensation of energy after exposure to stress, leading to the disease onset. With the myelination maturation, the energy needs are reduced; therefore the WM may better tolerate infection and other stress factors. However, because of the small number of cases and short time of follow-up after the first visit, we could not exclude that patients with “stabilized pattern” may have further attacks.

Limitations of the study

There are some limitations in this study: (1) we did not perform respiratory chain enzyme assay because muscle biopsies were not available in these patients. (2) Functional study on the variants was lacking; we used the variant interpretation guidelines of the American College of Medical Genetics and Genomics to assign the pathogenicity of the candidate variants. Further investigations are needed.

Conclusions

In this study of 37 children sharing the common neuroimaging feature of WM cavities, we identified eight disease-causing genes. The study expanded the number of genes involved in CLEs to 22. Most of the reported genes were involved in mitochondrial function. *IBA57* is the most common candidate gene; it was identified in half of the children with CLEs. Most patients stabilized or improved after an acute or subacute onset, which is different from most other inherited metabolic diseases or leukodystrophies. More cases and a longer follow-up are needed to better understand CLEs.

Acknowledgements

This study was supported by National Science and Technology Major Project of the Ministry of Science and Technology of China (grant nos. 2017ZX09304029-006), National Key Research and Development Program of China (grant nos. 2016YFC0901505 and 2016YFC1306201), and Beijing Key Laboratory of Molecular Diagnosis and Study on Pediatric Genetic Diseases (grant no. BZ0317).

References

1. Parikh S, Bernard G, Leventer RJ, et al. A clinical approach to the diagnosis of patients with leukodystrophies and genetic leukoencephelopathies. Mol Genet Metab. 2015;4:501–515.
2. van der Knaap MS, Bugiani M. Leukodystrophies: a proposed classification system based on pathological changes and pathogenetic mechanisms. Acta Neuropathol. 2017;134:351–382.
3. SakkuBai N, Genila B, Doris L, et al. Progressive cavitating leukoencephalopathy: a novel childhood disease. Ann Neurol. 2005;58:929–938.
4. Björkman K, Sofou K, Darin N, et al. Broad phenotypic variability in patients with complex I deficiency due to mutations in NDUFS1 and NDUFV1. Mitochondrion. 2015;21:33–40.
5. Breningstall GN, Shoffner J, Patterson RJ. Siblings with leukoencephalopathy. Semin Pediatr Neurol. 2008;15:212–215.
6. Ortega-Recalde O, Fonseca DJ, Patiño LC, et al. A novel familial case of diffuse leukodystrophy related to NDUFV1 compound heterozygous mutations. Mitochondrion. 2013;13:749–754.
7. Kevelam SH, Rodenburg RJ, Wolf NI, et al. NUBPL mutations in patients with complex I deficiency and a distinct MRI pattern. Neurology. 2013;17:1577–1583.
8. Valente L, Tiranti V, Marsano RM, et al. Infantile encephalopathy and defective mitochondrial DNA translation in patients with mutations of mitochondrial elongation factors EFG1 and EFTu. Am J Hum Genet. 2007;1:44–58.
9. Ghezzi D, Goffrini P, Uziel G, et al. SDHAF1, encoding a LYR complex-II specific assembly factor, is mutated in SDH-defective infantile leukoencephalopathy. Nat Genet. 2009;6:654–656.
10. Oláhová M, Hardy SA, Hall J, et al. LRPPRC mutations cause early-onset multisystem mitochondrial disease outside of the French-Canadian population. Brain. 2015;12:3503–3519.
11. Massa V1, Fernandez-Vizarra E, Alshahwan S, et al. Severe infantile encephalomyopathy caused by a mutation in COX6B1, a nucleus-encoded subunit of cytochrome c oxidase. Am J Hum Genet. 2008;6:1281–1289.
12. Kashani A, Thiffault I, Dilenge ME, et al. A homozygous mutation in the NDUFS1 gene presents with a mild cavitating leukoencephalopathy. Neurogenetics. 2014;15:161–164.
13. Ferreira M, Torraco A, Rizza T, et al. Progressive cavitating leukoencephalopathy associated with respiratory chain complex I deficiency and a novel mutation in NDUFS1. Neurogenetics. 2011;12:9–17.
14. Invernizzi F, Ardissone A, Lamantea E, et al. Cavitating leukoencephalopathy with multiple mitochondrial dysfunction syndrome and NFU1 mutations. Front Genet. 2014;5:412.
15. Biancheri R, Rossi D, Cassandrini D. Cavitating leukoencephalopathy in a child carrying the mitochondrial A8344G mutation. AJNR Am J Neuroradiol. 2010;9:E78–E79.
16. Martinez Lyons A, Ardissone A, Reyes A, et al. COA7 (C1orf163/RESA1) mutations associated with mitochondrial leukoencephalopathy and cytochrome c oxidase deficiency. J Med Genet. 2016;12:846–849.
17. Pippucci T, Maresca A, Magini P, et al. Homozygous NOTCH3 null mutation and impaired NOTCH3 signaling in recessive early-onset arteriopathy and cavitating leukoencephalopathy. EMBO Mol Med. 2015;6:848–858.
18. Dallabona C, Abbink TE, Carrozzo R, et al. LYRM7 mutations cause a multifocal cavitating leukoencephalopathy with distinct MRI appearance. Brain. 2016;3:782–794.
19. Invernizzi F, Tigano M, Dallabona C, et al. A homozygous mutation in LYRM7/MZM1L associated with early onset encephalopathy, lactic acidosis, and severe reduction of mitochondrial complex III activity. Hum Mutat. 2013;34:1619–1622.
20. Hempel M, Kremer LS, Tsiakas K, et al. LYRM7—associated complex III deficiency: a clinical, molecular genetic, MR tomographic, and biochemical study. Mitochondrion. 2017;37:55–61.
21. Melchionda L, Haack TB, Hardy S, et al. Mutations in APOPT1, encoding a mitochondrial protein, cause cavitating leukoencephalopathy with cytochrome c oxidase deficiency. Am J Hum Genet. 2014;3:315–325.
22. Liu M, Zhang J, Zhang Z, et al. Phenotypic spectrum of mutations in IBA57, a candidate gene for cavitating leukoencephalopathy. Clin Genet. 2018;93:235–241.
23. Ishiyama A, Sakai C, Matsushima Y, et al. IBA57 mutations abrogate iron-sulfur cluster assembly leading to cavitating leukoencephalopathy. Neurol Genet. 2017;3:e184.
24. Torraco A, Ardissone A, Invernizzi F, et al. Novel mutations in IBA57 are associated with leukodystrophy and variable clinical phenotypes. J Neurol. 2016;264:102–111.
25. Alston CL, Davison JE, Meloni F, et al. Recessive germline SDHA and SDHB mutations causing leukodystrophy and isolated mitochondrial complex II deficiency. J Med Genet. 2012;49:569–577.

26. Ishiyama A, Muramatsu K, Uchino S, et al. NDUFAF3 variants that disrupt mitochondrial complex I assembly may associate with cavitating leukoencephalopathy. Clin Genet. 2018;93:1103–1106.
27. Rubegni A, Ferrari AR, Pasquariello R, et al. Relapsing-remitting course of cystic leukoencephalopathy. Pediatr Neurol. 2018;89:63–65.
28. Gerards M, Sluiter W, van den Bosch BJ, et al. Defective complex I assembly due to C20orf7 mutations as a new cause of Leigh syndrome. J Med Genet. 2010;47:507–512.
29. Piekutowska-Abramczuk D, Assouline Z, Mataković L, et al. NDUFB8 mutations cause mitochondrial complex I deficiency in individuals with Leigh-like encephalomyopathy. Am J Hum Genet. 2018;102:460–467.
30. Bénit P, Beugnot R, Chretien D, et al. Mutant NDUFV2 subunit of mitochondrial complex I causes early onset hypertrophic cardiomyopathy and encephalopathy. Hum Mutat. 2003;6:582–586.
31. Cameron JM, MacKay N, Feigenbaum A, et al. Exome sequencing identifies complex I NDUFV2 mutations as a novel cause of Leigh syndrome. Eur J Paediatr Neurol. 2015;5:525–532.
32. Joost K, Rodenburg R, Piirsoo A, et al. A novel mutation in the SCO2 gene in a neonate with early-onset cardioencephalomyopathy. Pediatr Neurol. 2010;42:227–230.
33. Baker PR, Friederich MW, Swanson MA, et al. Variant non ketotic hyperglycinemia is caused by mutations in LIAS, BOLA3 and the novel gene GLRX5. Brain. 2014;137:366–379.